

Complicated mechanism of softening in vanadium at high pressures

Qiumin Jing,^{*} Lei Liu[†], Huayun Geng, Feng Xi, Hao Wang, Jun Li, Yi Zhang[✉], Shourui Li, Junjie Gao, Xiaohui Chen, Yuying Yu, and Qiang Wu

National Key Laboratory of Shock Wave and Detonation Physics, Institute of Fluid Physics, CAEP, Mianyang 621900, Sichuan, China



(Received 10 March 2024; revised 3 April 2024; accepted 8 April 2024; published 3 May 2024)

The mechanical properties of materials at high pressures determine their applications in extreme conditions. Vanadium, a rare-earth metal, exhibits abnormal strength softening at high pressures. However, the mechanism of this remarkable softening is still open to debate up to now. In the present study, the dislocation density, elastic modulus, and lattice distortion effects on the strength of vanadium at high pressure are investigated systematically. The *in situ* dislocation density of vanadium as a function of pressure is measured. It is demonstrated that the softening mechanism of vanadium is multifaceted: the elastic modulus softening, the anomalous decrease of dislocation density, and the body-centered-cubic lattice distortion all contribute to the strength softening of vanadium. Among these factors, the elastic modulus softening is the dominant one and the abrupt drop of dislocation density has a moderate influence, while the body-centered-cubic lattice distortion has an inappreciable contribution to the anomalous strength softening of vanadium. This work highlights the general factors that affect the strengthening and softening mechanism of materials under extreme conditions.

DOI: [10.1103/PhysRevB.109.184104](https://doi.org/10.1103/PhysRevB.109.184104)

I. INTRODUCTION

Vanadium, a transition-metal element of the fifth subgroup (VB) with a body-centered-cubic (bcc) structure (space group $Im-3m$), has a broad spectrum of technological applications. Vanadium-based alloys are considered a potential cover and shielding wall of fusion reactors [1] owing to their small neutron capture area, excellent corrosion resistance, and good creep strength at high temperatures. Vanadium is an important alloying element additive in the steel metallurgy industry [2], in which it can effectively increase the strength, toughness, and ductility of iron. In the aerospace industry, a small amount of vanadium plays an important role as a strengthening agent and stabilizer in titanium alloy [3]. Vanadium is also used as a catalyst [4] in the chemical industry. In addition, vanadium is an indispensable ingredient in producing colorants [5], vanadium batteries [6], vanadium nanomaterials [7], and vanadium thin films [8].

Vanadium yet remains poorly understood from a physical point of view to date. In past decades, continuous efforts have been devoted to grasp the engineering complexities of vanadium, because it does not behave like a normal metal at high pressure, especially the mechanical behaviors. For example, pure vanadium exhibits a significant and continuous strength softening from 52.9 to 90 GPa [9]. This behavior of vanadium is quite a contrast to general metals, which gain strength and ductility enhancement if small amounts of load or pressure are applied, as Bridgman [10] observed around a century ago. Klepeis *et al.* [9] became aware of the similarity between the strength-pressure relationship and the predicted

pressure dependence of the shear modulus of vanadium, thus considering that the structure transformation was responsible for the abnormal softening of vanadium. First-principles calculations [11–13] discovered that the shear modulus of vanadium softened drastically at high pressures, and even got a negative value which induced the instability of the bcc lattice and consequently triggered the bcc-to-rhombohedral structural phase transition. This bcc-to-rhombohedral structure transformation was confirmed by later static high-pressure experiments [14,15], indicated by the asymmetric broadening of the (110) reflection. However, very recently, theoretical and experimental investigations [16–20] discovered that the bcc phase was stable above 50 GPa and the rhombohedral structure was a metastable phase. The asymmetric broadening of the (110) reflection arises from the subtle lattice distortions from cubic symmetry induced by the nonhydrostatic pressure in the sample chamber of a diamond anvil cell (DAC, widely used to generate static high pressures). The experimentally observed rhombohedral phase [14,15] is far from being perfect and should be interpreted as a kind of lattice distortion rather than a phase transition. A similar but less conspicuous strength softening was also observed in the same VB group elements Ta [21,22] and Nb [23]. Researchers assigned the possible material damage, unusual softening of the microscopic deviatoric strain, and the shear modulus softening to the strength softening of those VB group metals. This complicated strength softening mechanism in VB metals makes the fundamental understanding of their mechanical behavior ambiguous and calls for further investigations.

Yield strength, the minimum stress necessary to induce the plastic deformation of materials, is strictly defined as flow stress once suffering over much plastic strain. According to strengthening mechanisms of polycrystalline metals, the flow stress (σ_y) is the summation of the lattice friction stress (σ_{fr})

^{*}Corresponding author: j_qm@163.com

[†]Corresponding author: lei.liu@caep.cn

and the contributions from various incremental strengthening mechanisms [including dislocation strengthening ($\Delta\sigma_\rho$), grain boundary strengthening ($\Delta\sigma_{gb}$), stack fault strengthening ($\Delta\sigma_{sf}$), and phase-transformation-induced strengthening ($\Delta\sigma_{pht}$)] under static loading. The pressure strengthening is included in the lattice friction stress. To reveal the softening mechanism, it is necessary to investigate individual contributions systematically, especially the microstructure and dislocation density.

Direct measurement methods of dislocation density and microstructure cluster around transmission electron microscopy (TEM) [24,25]. Nevertheless, in the case of a severely compressed vanadium sample at high pressure (usually with a dislocation density higher than 10^{14} m^{-2}), it is challenging to observe dislocations and carry out Burgers vector analysis by conventional TEM because the sample is encapsulated by the diamond anvils and metallic gasket in the DAC [26]. Furthermore, for a heterogeneous system where the dislocation density fluctuates within a grain in a submicron scale, the TEM results just present a microscopic local dislocation density [27]. Benefiting from the tremendous advances of synchrotron-related techniques in the past two decades, we have the capability to measure the diffraction profiles of materials with high accuracy. Accordingly, the x-ray diffraction (XRD) line profile analysis method [28–30] offers a powerful and promising alternative tool for dislocation density measurement, especially in highly deformed metals. The XRD line profile analysis method provides a macroscopic average value for heterogeneous systems and can overcome the limit of TEM up to $5 \times 10^{14} \text{ m}^{-2}$ local densities by weak beam techniques [29]. In the pioneering *in situ* measurement of dislocation density at high pressures, Nisr *et al.* [31] used the high-resolution three-dimensional x-ray diffraction technique and x-ray line profile analysis to characterize the dislocations in grains of MgGeO_3 post-perovskite up to 90 GPa. However, as far as the authors are concerned, there are still no experimental reports on the *in situ* study of the dislocation density and flow stress of materials simultaneously at high pressures.

In the present work, the *in situ* dislocation density and flow stress of vanadium were determined simultaneously by performing an XRD line profile broadening analysis up to 62.4 GPa at room temperature. The dislocation density is directly associated with the macroscopic strength. An apparent strength softening was discovered and the multifaceted strength softening mechanism was discussed thoroughly.

II. METHODS

A. Synchrotron-based x-ray diffraction

High pressure was generated using a modified Mao-Bell-type symmetric DAC with a pair of diamond anvils with culets size of 200 μm . The rhenium gasket with an initial thickness of 250 μm was indented to around 30 μm . A laser-drilled hole in the center of the preindented region served as a sample chamber. The vanadium powder (purity 99.5%, -325 mesh, Alfa Aesar) was loaded into the sample chamber directly. For maintaining a strict stress state and measuring clean diffraction patterns, neither a pressure medium nor a pressure scale was used. So, the sample stress condition is

highly nonhydrostatic according to a recent study [32]. Pressure in the sample chamber was calculated according to the equation of state of vanadium [14]. The pressure uncertainty originates from the measured uncertainty of the unit cell volume and the uncertainty of the vanadium pressure scale used [14]. The pressure discrepancies among different pressure scales are discussed in detail in the Supplemental Material [33] (see also Refs. [34–41] therein). The present calculated bulk modulus and its pressure derivative are also compared with the previous studies in Ref. [33]. The synchrotron-based XRD experiments were performed at the 4W2 beamline of the Beijing Synchrotron Radiation Facility (BSRF) at room temperature. Monochromatic x-ray with a wavelength of 0.6199 \AA (20 keV) was collimated to several micrometers and then illuminated on the sample. The diffraction signal was collected by a Pilatus charge-coupled device (1475×1679 pixels with a pixel size of $172 \times 172 \mu\text{m}^2$) detector. The CeO_2 and LaB_6 references from NIST were used to calibrate the distance from sample to detector, the tilt of the detector, and the instrumental broadening, respectively. The two-dimensional (2D) diffraction images were integrated using the Dioptas [42] software to acquire the 2θ intensity curves, which were further fitted with a type-I Voigt function. The fittings yield peak positions for pressure measurement according to the equation of state of vanadium [14], and the full width at half maximum (FWHM) for yield strength or flow stress (Sec. II C) [37–39] and dislocation density analysis (Sec. II D) [28–30].

B. Theoretical calculations

The elastic constants of vanadium were calculated using the energy-strain method [43,44]. The energy calculation was carried out by using the VASP package based on density functional theory (DFT) [45,46]. A plane-wave basis set was employed with a kinetic energy cutoff of 900 eV. The electron-core interaction was described by a projector-augmented wave (PAW) pseudopotential [47] containing 13 valence electrons (including $3s^2$, $3p^6$, $3d^3$, and $4s^2$ states). The electron exchange correlation was handled by a generalized gradient approximation with the Perdew-Berke-Ernzerhof (PBE) parametrization [48]. The Monkhorst-Pack (MP) grid with a size of $30 \times 30 \times 30$ was adopted for K -point sampling. The self-consistent field (SCF) convergence tolerance was set as 10^{-8} eV/cell (0.001 eV/ \AA) for energy (force), respectively.

C. Broadening analysis method

The stress of a polycrystalline sample nonhydrostatically compressed is generally considered a superposition of microscopic deviatoric stress and macroscopic differential stress [37], which result in micro- and macrostrains, respectively. The microscopic strain causes the broadening of the diffraction lines and the macroscopic one leads to the shift of diffraction lines. The x-ray diffraction line profile and the peak broadening are used to characterize the microstructure and dislocation density [28–30] of materials. In addition, the diffraction peak broadening is used to analyze the microstrain and then the yield strength and flow stress [37–41].

The yield strength or flow stress was determined by the diffraction line broadening analysis method. For anisotropic

materials, the diffraction line broadening due to microstrain and crystallite size varies with diffraction angle under angle-dispersive x-ray diffraction geometry as [41]

$$(2w_{hkl} \cos\theta_{hkl})^2 = (\lambda/D)^2 + (4\nu)^2[\sin^2\theta_{hkl}/E(hkl)^2], \quad (1)$$

where $2w_{hkl}$ is the FWHM of the peak from the (hkl) reflections at the Bragg angle of $2\theta_{hkl}$. λ , D , ν , and E_{hkl} are the wavelength of the incident x-ray, grain size, microscopic deviatoric stress, and single-crystal Young's modulus, respectively. ν can be extracted from the slope of the $(2\omega_{hkl} \cos\theta_{hkl})^2$ vs $[\sin^2\theta_{hkl}/E(hkl)^2]$ plot (the so-called Γ plot). Once the polycrystalline sample yields and suffers plastic deformation, ν can be interpreted as the yield strength or flow stress. A detailed analysis method is presented in Ref. [33].

D. Modified Williamson-Hall and modified Warren-Averbach methods

The dislocation density was analyzed by combining the modified Williamson-Hall (MWH) and the modified Warren-Averbach (MWA) methods [30]. The MWH equation approximates the dislocation density from x-ray peak broadening as follows:

$$\Delta K \cong 0.9/D + bM\sqrt{\pi/2\rho}(K\bar{C}^{1/2}), \quad (2)$$

where ΔK is the peak width, D is the so-called apparent size parameter or crystallite size, b is the magnitude of the Burgers vector, M is a dimensionless constant known as the dislocation distribution parameter, ρ is the dislocation density, K is the magnitude of the diffraction vector, and \bar{C} is the average contrast factor of dislocations and is a function of the Miller indices. The detailed analysis of \bar{C} can be found in Ref. [33].

It should be noted that the MWH method only uses the linewidth information and cannot give ρ and M separately. It is needed to combine the MWA method [30] to determine ρ and M independently. In the MWA method, the measured diffraction pattern is expressed as a Fourier series and the dislocation density can be obtained by using

$$\ln A(L) \cong \ln A^S(L) - \rho \frac{\pi b^2}{2} L^2 \ln \frac{R_e}{L} K^2 \bar{C} + O(K^2 \bar{C}), \quad (3)$$

where $A(L)$ is the real part of the cosine Fourier coefficient of the (hkl) diffraction profile depending on the Fourier length L ; L is the undistorted distance between a pair of cells along the a_3 direction and given as $L = na_3$, where n represents the integers starting from zero and $a_3 = \lambda/[2(\sin\theta_2 - \sin\theta_1)]$, in which $(\theta_2 - \theta_1)$ is the angular range of the measured diffraction profile. A^S is the size of the Fourier coefficient, and O represents higher-order terms of $K^2 \bar{C}$. By fitting $\ln A(L)$ as a quadratic function of $K^2 \bar{C}$ and $A^S(L)$, the slope $X(L)$ can be written as

$$\frac{X(L)}{L^2} = \rho \frac{\pi b^2}{2} (\ln R_e - \ln L). \quad (4)$$

From the linear regression of $X(L)/L^2$ and $\ln L$, the dislocation density ρ and the effective outer cutoff radius of dislocation, R_e , can be determined. By combining the MWH and MWA methods, the dislocation distribution parameter M can also be calculated.

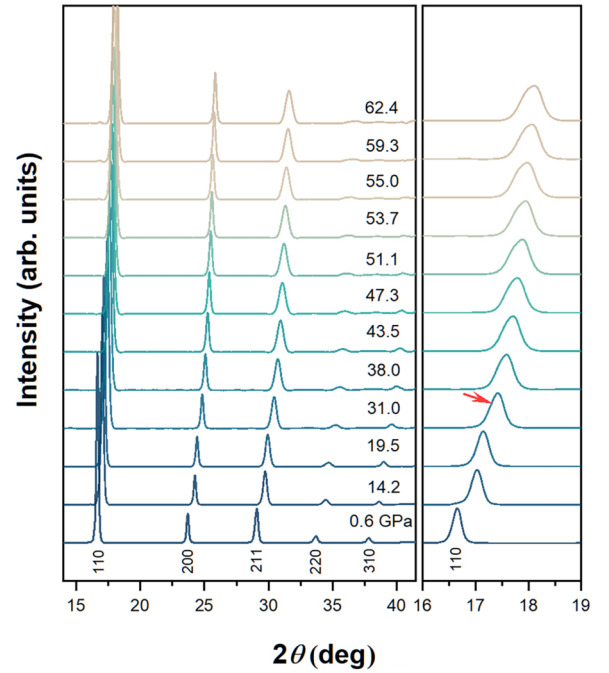


FIG. 1. XRD patterns of vanadium collected during compression using synchrotron radiation with a wavelength of 0.6199 Å (20 keV). The Miller indices of corresponding reflections are indicated in the figure. The right-hand panel enlarges the broadening of bcc (110) peaks and the arrow indicates the commencement of the splitting of the (110) peak.

III. RESULTS AND DISCUSSIONS

A. XRD results

Figure 1 presents the x-ray diffraction profiles of vanadium integrated from the 2D patterns at high pressures. The right-hand panel in Fig. 1 enlarges the (110) reflections of the bcc structure, which indicates notable peak broadening at high pressure arising from the strain increasing and/or grain size decreasing. A slight asymmetric feature of the (110) reflections emerges at 31.0(3) GPa, which is consistent with the previous results under nonhydrostatic compression (~ 30 GPa reported by Jenei *et al.* [15] and ~ 27 – 32 GPa by Xiong and Liu [49]). The FWHM of the (110) reflections as a function of pressure is presented in Fig. 2. Following an initial increase, a much-pronounced increase in the FWHM of the (110) reflection was observed between 31.0(5) and 43.5(5) GPa. This slope change may originate from the lattice distortion. Above 43.5(5) GPa, the recovery from the distorted bcc phase leads to a decrease of the slope.

B. Anomalous strength softening of vanadium

Figure 3 shows the typical Γ plots of vanadium at selected pressures. The flow stress can be directly extracted from the slopes of the fitting lines of Γ plots. The instrumental broadening is small compared to the peak width of vanadium and leads to a negligible effect on the strength of materials, especially at high pressures. The elastic constants needed to obtain the flow stress according to Eq. (3) are calculated by the first-principles method and shown in Fig. 4 (also see Ref. [33]). According

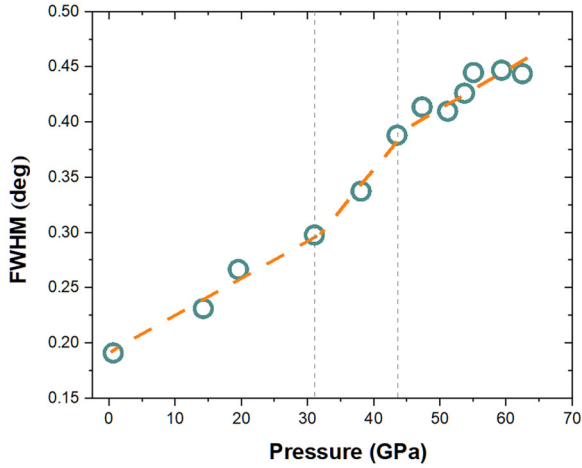


FIG. 2. FWHM of bcc (110) peak as a function of pressure. Dashed lines are a guide to the eye.

to the Born-Huang stability criteria [50], bcc vanadium is dynamically stable up to the highest pressure of the present research. The elastic constants at 0 GPa are listed in Table I compared with the previously calculated [35,51] and experimental [52] results. All the results show good consistency.

The deduced flow stresses of vanadium as a function of pressure are shown in Fig. 5. The pressure error bars are smaller than the symbol size. The results from Klepeis *et al.* [9] using the pressure gradient (PG) method and Xiong *et al.* [49] using the radial x-ray diffraction (RXRD) technique are

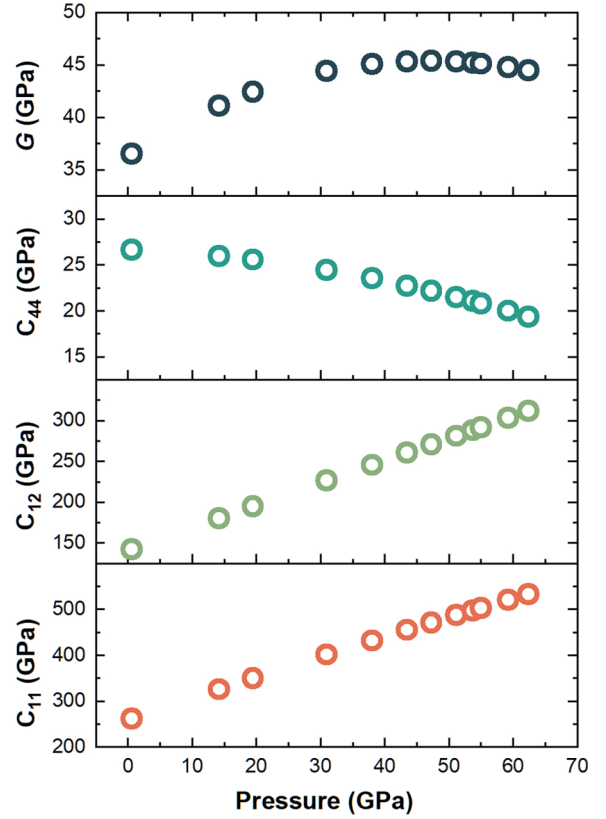


FIG. 4. The calculated elastic moduli of vanadium as a function of pressure.

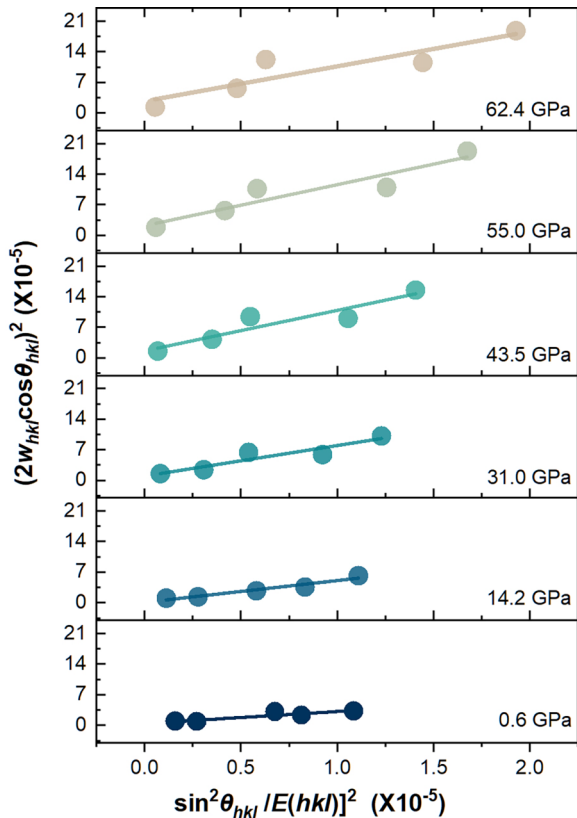


FIG. 3. The Γ plot at selected pressures.

also presented in Fig. 5 for comparison. Considering the intrinsic discrepancy in strength between the powder and the foil samples, Fig. 5 only illustrates the result of the powder sample measured by Klepeis *et al.*

Two distinct regimes in the flow stress of vanadium as a function of pressure are observed in Fig. 5. The flow stress increases with pressure up to 51.1(6) GPa first, arising from the pressure strengthening effect as observed in normal materials. As the pressure increases further, the flow stress decreases up to the highest experimental pressure of 62.4(7) GPa. Below 20.0(2) GPa, the flow stress agrees with the results from the PG method [9], which are much larger than those measured by the RXRD method [49]. The RXRD method determines the macroscopic differential strain, so the measured differential stress between the axial and radial directions would increase from the initial 0 GPa in the DAC, which would lead to a smaller “flow stress” at

TABLE I. The elastic modulus from various investigations at 0 GPa and temperature.

Ref.	Elastic modulus (GPa)				
	C_{11}	C_{12}	C_{44}	G	E
This work	269.65	139.34	25.46	37.5	105.2
Landa <i>et al.</i> [51]			30		
Koci <i>et al.</i> [35]	260	135	17.1		
Greiner <i>et al.</i> [52]	235.89	120.76	46.55	47.4	129.1

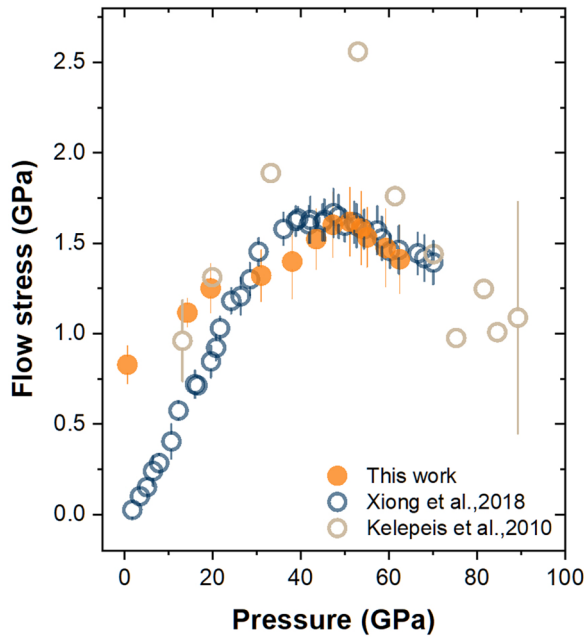


FIG. 5. The flow stress of vanadium as a function of pressure. The open circles denote the data from Xiong and Liu [49] and the results of the powder sample from Klepeis *et al.* [9]. The typical error bars of the PG method are presented at the lowest pressure and highest pressure, respectively. The pressure error bars of the present measurement are smaller than the symbol size.

relatively low pressures. Between 20.0(2) and 53.7(6) GPa, the flow stress coincides with that measured by the RXRD method [49], while the results from the PG method [5] give much larger values. In the PG method, the diamond culets usually undergo cupping deformation [53] at high pressure, which leads to an overestimate of the sample thickness and so too the flow stress. Above 53.7(6) GPa, all experimental results accord with each other and show a uniform trend by extrapolation. Notwithstanding the visible discrepancy between the different methods, an evident strength softening was discovered in all the experimental results despite different techniques being employed. The flow stress as a function of pressure reaches a maximum at 51.1 GPa, which is in reasonable agreement with the previous results (52.9 GPa by the PG method [9] and 47.4 GPa by the RXRD method [49]). The discrepancy of the onset pressures of softening originates from the different pressure scales used. Based on a series of shock reverse-impact experiments, Yu *et al.* [54] discovered a continuous increase of strength in vanadium with pressure, which is in contrast to the results from all the DAC experiments. This difference may originate from the high loading rate in the shock experiment and a strong rate-related hardening effect.

To resolve the long-standing melting controversy of Ta metal, Wu *et al.* [55] proposed a thermal-activated and shear-induced plastic flow of Ta before melting. According to their results, the yield stress of bcc metals turns out to be the threshold stress of this plastic flow, which is predicted to occur at high temperatures once the shear stress in the sample chamber of the DAC exceeds the sample's yield stress. Consequently, one can expect that vanadium is prone to transform

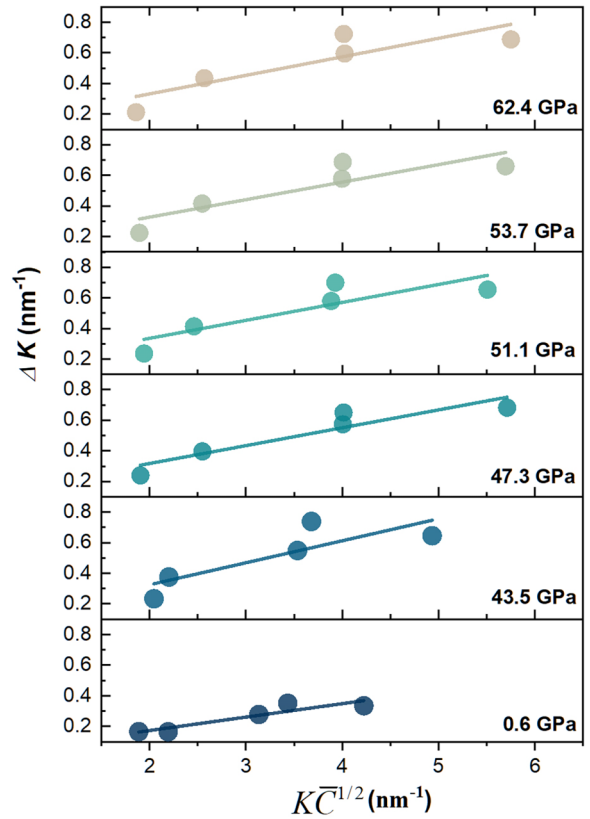


FIG. 6. The MWH plots of the FWHM for selected pressures according to Eq. (2).

into a plastic flow at high pressure because of the discovered pressure-induced softening of vanadium. This offers a plausible reason for the flat melting curve of vanadium measured using the speckle motion method [56].

C. Dislocation density decrease

The modified Williamson-Hall plots at selected pressures are shown in Fig. 6. The XRD peak broadening from the instrument was measured using the diffraction pattern of LaB₆ reference, which was subsequently subtracted from the XRD peak width. Since the intercepts and the slopes of the modified Williamson-Hall plots are proportional to the reciprocals of crystallite size and the microstrain, respectively, the crystallite size D and the product of $M\rho^{1/2}$ can be determined consequently. Figure 7(a) shows the MWA plot [$\ln A(L)$ versus $K^2\bar{C}$ at different Fourier length L] of vanadium at 62.4(7) GPa. By fitting $\ln A(L)$ with a quadratic function of $K^2\bar{C}$, the slope $X(L)$ can be determined. From the linear regression of $X(L)/L^2$ and $\ln L$, the dislocation density ρ and the effective outer cutoff radius of dislocation, R_e , can be obtained. Figure 7(b) shows the linear regression of $X(L)/L^2$ versus $\ln L$ at 62.4(7) GPa and the dislocation density is $1.61(26) \times 10^{15} \text{ m}^{-2}$.

Figure 8 shows the measured dislocation density of vanadium as a function of pressure. The dislocation density increases monotonously with pressure from $0.59(8) \times 10^{15} \text{ m}^{-2}$ at 0.6(1) GPa to $2.16(40) \times 10^{15} \text{ m}^{-2}$ at 43.5(5) GPa. However, a pronounced dislocation density reduction of $\sim 33\%$ from $2.16(40) \times 10^{15} \text{ m}^{-2}$ to $1.44(16) \times 10^{15} \text{ m}^{-2}$ is

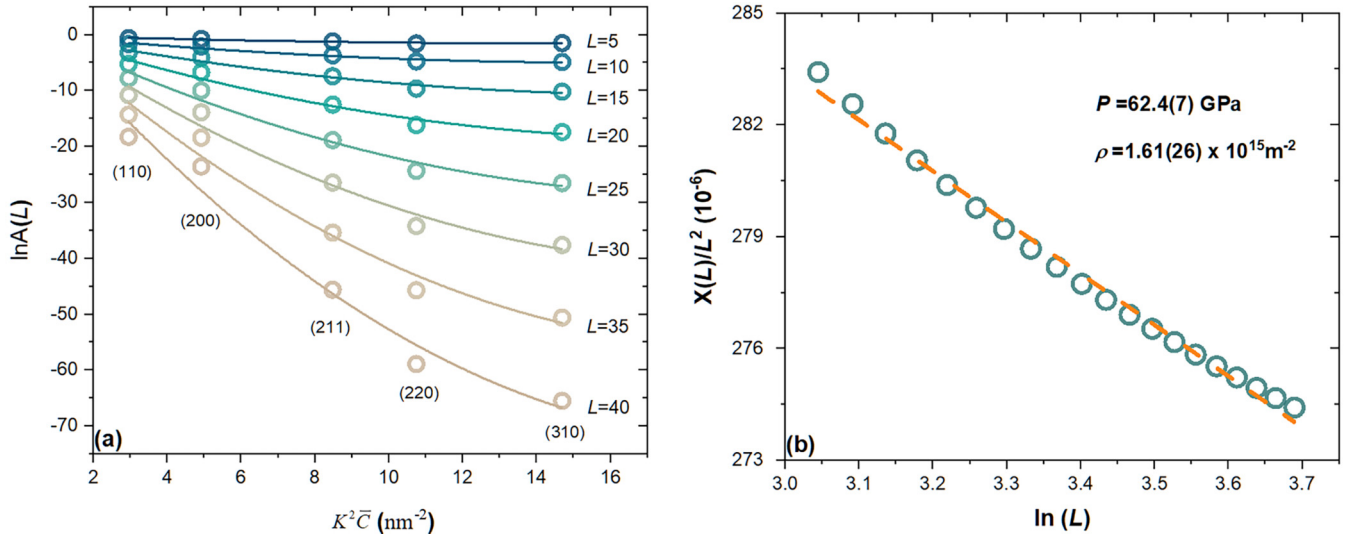


FIG. 7. (a) The MWA plot of Fourier coefficients for different Fourier lengths L according to Eq. (3) and (b) the linear regression of $X(L)/L^2$ and $\ln L$ according to Eq. (4) at 62.4(7) GPa. The Miller indices are indicated in the figure.

observed at 47.3(5) GPa. The abrupt reduction of the dislocation density originates from the partial dynamic recovery of dislocation induced by the local microstress relaxation during the distorted bcc lattice evolution at high pressures. Above 47.3(5) GPa, the dislocation density continues to increase with pressure again and reaches $1.61(26) \times 10^{15} \text{ m}^{-2}$ at the highest experimental pressure of 62.4(7) GPa.

D. Multifaceted softening mechanism

For pure vanadium, if the stacking fault is not taken into account at room temperature, the major contributions of the overall high-pressure flow stress include the friction stress σ_{fr} , the dislocation strengthening $\Delta\sigma_{\rho}$, and the grain boundary strengthening $\Delta\sigma_{\text{gb}}$. The lattice friction stress σ_{fr} resistant to the dislocation glide can be estimated by the Steinberg constitutive model [57], in which the shear modulus sets a natural scale for strength. Consequently, the pressure dependence of

yield strength follows the trend of the pressure dependence of shear modulus (shown in Fig. 4); thus it is expected that vanadium exhibits a continuous friction stress reduction above 47.3 GPa.

The dislocation strengthening $\Delta\sigma_{\rho}$ (strain hardening) arises from the intersection of dislocations during deformation in relatively larger grains and can be estimated using the Taylor equation $\Delta\sigma_{\rho} = \alpha M' G b \rho^{0.5}$ [58,59]. M' is the Taylor factor, which is 3.06 for bcc metals. α is a geometrical factor specific to the material that depends on the type and arrangement of the interacting dislocations. Strictly, α usually decreases with increasing deformation. In this work, α is approximately taken to be 0.3 at the initial pressure and 0.2 in the highest pressure due to an increasingly heterogeneous dislocation pattern [60], and linear interpolation is applied to obtain the values within the intermediate pressure. G is the shear modulus (shown in Fig. 4). The estimated dislocation strengthening contribution $\Delta\sigma_{\rho}$ is presented in Fig. 9.

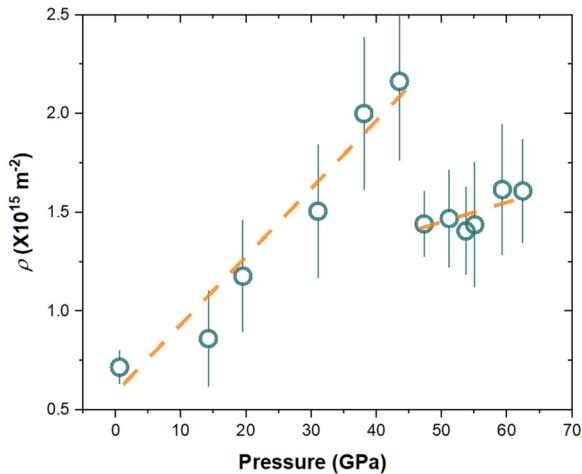


FIG. 8. Dislocation density of vanadium as a function of pressure at 300 K. The dashed lines are a guide to the eye.

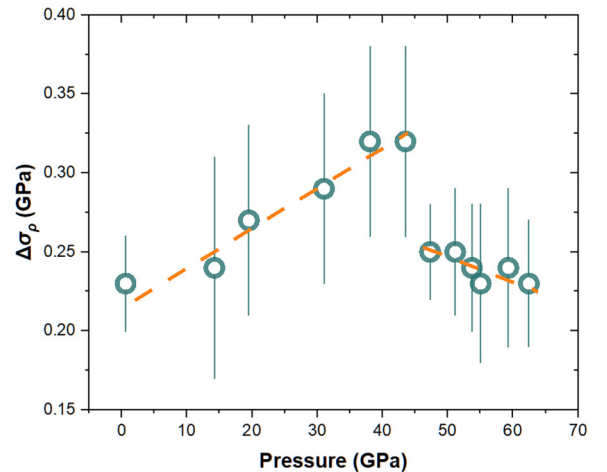


FIG. 9. The dislocation strengthening contribution of vanadium as a function of pressure.

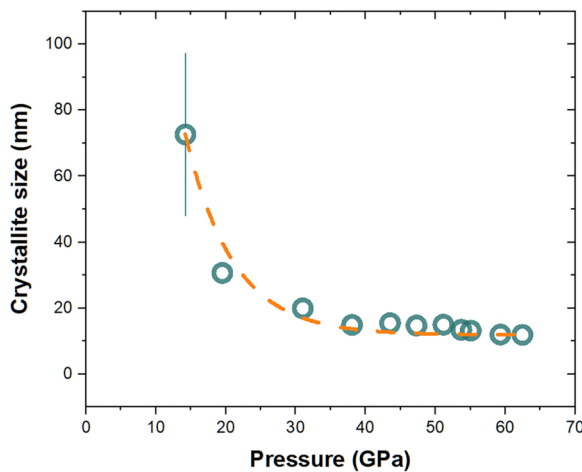


FIG. 10. The crystallite size dependent on pressure. The typical error bars of the crystallite size are presented at the lowest pressure.

An obvious drop of $\Delta\sigma_p$ is observed above 43.5(5) GPa, originating from the dramatic decrease of the dislocation density above 43.5(5) GPa (see Fig. 8) according to the Taylor equation because the shear modulus G and the lattice parameter a (subsequently the Burgers vector b) increase and decrease continuously with pressure, without any kinks. However, the overall flow stress did not show an abrupt decrease above 43.5(5) GPa, because the dislocation strengthening contributes only a small part, $\sim 17\text{--}26\%$.

The grain boundary strengthening (Hall-Petch strengthening) $\Delta\sigma_{gb}$ is grain size dependent and can be estimated by the Hall-Petch relationship [61] $\Delta\sigma_{gb} = k_{HP}/d_b^{0.5}$. K_{HP} is the Hall-Petch constant and d_b is the average grain size. To the authors' knowledge, the Hall-Petch constant data are not available in the literature. It should be noted that the crystallite size D given by the MWH and MWA methods represents the coherent scattering domain size [29], which is not directly related to dislocation densities or distance between dislocations and is far smaller than grain size. Only in nanocrystalline materials can the crystallite size coincide with grain size. Notwithstanding the lack of grain size in the literature, the crystallite size dependence on pressure is similar to grain size. Figure 10 indicates the pressure dependence of crystallite size. We can expect a similar trend in the pressure dependence of grain size. Consequently, the grain boundary strengthening increases with pressure and does not contribute to the strength softening according to the Hall-Petch relationship.

It should be noted that we observed a relatively slower increasing rate of the flow stress with pressure between 31.0(3) GPa and 43.5(5) GPa (see Fig. 5). But the change of the flow stress with pressure is continuous and quite different from that in conventional structure transformation materials,

such as $\alpha \rightarrow \omega$ of Zr [62], $\alpha \rightarrow \varepsilon$ of Fe [63], and B1 \rightarrow B2 of NaCl [64]. These materials have an evident volume collapse across phase boundaries, accompanying an abrupt strength enhancement [62,63] or decrease [64]. From this point of view, we are inclined to consider that vanadium does not undergo a structural phase transition in the range 31.0(3)–43.5(5) GPa. The slight strength changes of vanadium between 31.0(3) and 43.5(5) GPa may be a result of the fact that the distorted bcc structure has a relatively weaker strength.

Therefore, the strength softening of vanadium at high pressure mainly originates from the decreasing of friction stress and the anomalous decreasing of the dislocation strengthening. The decreasing friction stress arises from the softening of the shear modulus above 47.3(5) GPa. The reduction of the dislocation strengthening contribution originates from the softening of the shear modulus and the decreasing of the Burgers vector with pressures. The evolution of the distorted bcc lattice at high pressure leads to a dramatic drop in the dislocation density due to a microstress relaxation. As the dislocation density contribution is a relatively smaller amount, the abrupt decrease of the dislocation density did not result in an obvious drop in the overall flow stress. Because of the coupling effect of the grain boundary strengthening, the strength softening did not directly follow the trend of the shear modulus but postponed to 51.1(6) GPa.

IV. CONCLUSIONS

In summary, we carried out room-temperature synchrotron x-ray diffraction measurements on vanadium powder compressed in a DAC apparatus. An obvious asymmetric broadening of (110) reflection indicates a slight distortion of bcc structure. By using the XRD line profile analysis, the dislocation density of vanadium was *in situ* measured up to 62.4(7) GPa. An abrupt drop of the dislocation density was observed above 43.5(5) GPa. A continuous strength softening was found above 51.1(6) GPa using the XRD peak broadening analysis. The strength softening in vanadium can be attributed to the combined effect of the shear modulus softening, dislocation density decreasing, and bcc lattice distortion. The shear modulus softening is the dominant factor while the bcc lattice distortion has a slight contribution to the anomalous softening of strength.

ACKNOWLEDGMENTS

Q. Jing is thankful for the helpful discussion with Dr. Zhijian Fan. This work was supported by the National Natural Science Foundation of China (Grants No. 11872056 and No. 12174356). The experiment was carried out with the support of the 4W2 beamline at Beijing Synchrotron Radiation Facility and BL15U1 beamline at Shanghai Synchrotron Radiation Facility.

- [1] J. M. Chen, V. M. Chernov, R. J. Kurtz, and T. Muroga, Overview of the vanadium alloy researches for fusion reactors, *J. Nucl. Mater.* **417**, 289 (2011).
- [2] Z. Oksiuta, M. Lewandowska, K. J. Kurzydowski, and N. Baluc, Effect of vanadium addition on the microstructure and

mechanical properties of the ODS ferritic steels, *J. Nucl. Mater.* **442**, S84 (2013).

- [3] Q. Wang, S. Hui, W. Ye, R. Liu, and X. Song, Quasi-static and dynamic plastic deformation behavior in titanium with vanadium addition, *Rare Met.* **42**, 2361 (2023).

- [4] Z. Lu, H. Yu, X. Lu, M. Song, F. Wu, J. Zheng, Z. Yuan, and L. Zhang, Two-dimensional vanadium nanosheets as a remarkably effective catalyst for hydrogen storage in MgH_2 , *Rare Met.* **40**, 3195 (2021).
- [5] R. G. McQueen and S. P. Marsh, Equation of state for nineteen metallic elements from shock-wave measurements to two megabars, *J. Appl. Phys.* **31**, 1253 (1960).
- [6] A. Trovo, M. Rugna, N. Poli, and M. Guarnieri, Prospects for industrial vanadium flow batteries, *Ceram. Int.* **49**, 24487 (2023).
- [7] F. Bei and Y. Li, Synthesis and characterization of coordination nano-material containing vanadium with helical structure, *Adv. Mater. Res.* **148–149**, 1507 (2011).
- [8] P. Guo, Z. Bieglerb, T. Back, and A. Sarangan, Vanadium dioxide phase change thin films produced by thermal oxidation of metallic vanadium, *Thin Solid Films* **707**, 138117 (2020).
- [9] J.-H. P. Klepeis, H. Cynn, W. J. Evans, R. E. Rudd, and L. H. Yang, Diamond anvil cell measurement of high-pressure yield strength of vanadium using *in situ* thickness determination, *Phys. Rev. B* **81**, 134107 (2010).
- [10] P. W. Bridgman, Effects of high shearing stress combined with high hydrostatic pressure, *Phys. Rev.* **48**, 825 (1935).
- [11] A. K. Verma and P. Modak, Structural phase transitions in vanadium under high pressure, *Europhys. Lett.* **81**, 37003 (2008).
- [12] S. L. Qiu and P. M. Marcus, Phases of vanadium under pressure investigated from first principles, *J. Phys.: Condens. Matter* **20**, 275218 (2008).
- [13] A. Landa, P. Söderlind, A. Ruban, O. E. Peil, and L. Vitos, Stability in bcc transition metals: Madelung and band-energy effects due to alloying, *Phys. Rev. Lett.* **103**, 235501 (2009).
- [14] Y. Ding, R. Ahuja, J. Shu, P. Chow, W. Luo, and H. K. Mao, Structural phase transition of vanadium at 69 GPa, *Phys. Rev. Lett.* **98**, 085502 (2007).
- [15] Z. Jenei, H. P. Liermann, H. Cynn, J.-H. P. Klepeis, B. J. Baer, and W. J. Evans, Structural phase transition in vanadium at high pressure and high temperature: Influence of nonhydrostatic conditions, *Phys. Rev. B* **83**, 054101 (2011).
- [16] Y. X. Wang, Q. Wu, X. R. Chen, and H. Y. Geng, Stability of rhombohedral phases in vanadium at high-pressure and high-temperature: First-principles investigations, *Sci. Rep.* **6**, 32419 (2016).
- [17] Y. Wang, H. Wu, Y. Liu, H. Wang, X. Chen, and H. Geng, Recent progress in phase stability and elastic anomalies of group VB transition metals, *Crystals* **12**, 1762 (2022).
- [18] Y. Akahama, S. Kawaguchi, N. Hirao, and Y. Ohishi, High-pressure stability of bcc-vanadium and phase transition to a rhombohedral structure at 200 GPa, *J. Appl. Phys.* **129**, 135902 (2021).
- [19] M. G. Stevenson, E. J. Pace, C. V. Storm, S. E. Finnegan, G. Garbarino, C. W. Wilson, D. McGonigle, S. G. Macleod, and M. I. McMahon, Pressure-induced bcc-rhombohedral phase transition in vanadium metal, *Phys. Rev. B* **103**, 134103 (2021).
- [20] D. Errandonea, S. G. MacLeod, L. Burakovsky, D. Santamaria-Perez, J. E. Proctor, H. Cynn, and M. Mezouar, Melting curve and phase diagram of vanadium under high-pressure and high-temperature conditions, *Phys. Rev. B* **100**, 094111 (2019).
- [21] S. T. Weir, J. Akella, C. Ruddle, T. Goodwin, and L. Hsiung, Static strengths of Ta and U under ultrahigh pressures, *Phys. Rev. B* **58**, 11258 (1998).
- [22] Q. Jing, Q. Wu, J. Xu, Y. Bi, L. Liu, S. Liu, Y. Zhang, and H. Geng, Anomalous softening of yield strength in tantalum at high pressures, *J. Appl. Phys.* **117**, 055903 (2015).
- [23] Q. Jing, Q. He, Y. Zhang, S. Li, L. Liu, Q. Hou, H. Geng, Y. Bi, Y. Yu, and Q. Wu, Unusual softening behavior of yield strength in niobium at high pressures, *Chin. Phys. B* **27**, 106201 (2018).
- [24] S. Morito, J. Nishikawa, and T. Maki, Dislocation density within lath Martensite in Fe-C and Fe-Ni alloys, *ISIJ Int.* **43**, 1475 (2003).
- [25] Z. Cong and Y. Murata, Dislocation density of lath martensite in 10Cr-5W heat-resistant steels, *Mater. Trans.* **52**, 2151 (2011).
- [26] W. A. Bassett, Diamond anvil cell, 50th birthday, *High Press. Res.* **29**, 163 (2009).
- [27] S. Takebayashi, T. Kunieda, N. Yoshinaga, K. Ushioda, and S. Ogata, Comparison of the dislocation density in martensitic steels evaluated by some x-ray diffraction methods, *ISIJ Int.* **50**, 875 (2010).
- [28] T. Ungár and A. Borbély, The effect of dislocation contrast on x-ray line broadening: A new approach to line profile analysis, *Appl. Phys. Lett.* **69**, 3173 (1996).
- [29] T. Ungár, Dislocation densities, arrangements and character from x-ray diffraction experiments, *Mater. Sci. Eng. A* **309**, 14 (2001).
- [30] F. HajyAkbar, J. Sietsma, A. J. Böttger, and M. J. Santofimia, An improved x-ray diffraction analysis method to characterize dislocation density in lath martensitic structures, *Mater. Sci. Eng. A* **639**, 208 (2015).
- [31] C. Nisr, G. Ribárik, T. Ungár, G. B. M. Vaughan, P. Cordier, and S. Merkel, High resolution three-dimensional x-ray diffraction study of dislocations in grains of MgGeO_3 post-perovskite at 90 GPa, *J. Geophys. Res.* **117**, B03201 (2012).
- [32] D. Errandonea, Y. Meng, M. Somayazulu, and D. Hausermann, Pressure-induced $\alpha \rightarrow \omega$ transition in titanium metal: A systematic study of the effects of uniaxial stress, *Physica B* **355**, 116 (2005).
- [33] See Supplemental Material at <http://link.aps.org/supplemental/10.1103/PhysRevB.109.184104> for pressure differences of different vanadium equations of state, broadening analysis method, MWH and MWA methods, and elastic constants of vanadium as a function of pressure.
- [34] Y. Wang, Y. Liu, Z. Yan, W. Liu, H. Geng, and X. Chen, Ab initio dynamical stability and lattice thermal conductivity of vanadium and niobium at high temperature, *Solid State Commun.* **323**, 114130 (2021).
- [35] L. Koci, Y. Ma, A. R. Oganov, P. Souvatzis, and R. Ahuja, Elasticity of the superconducting metals V, Nb, Ta, Mo, and W at high pressure, *Phys. Rev. B* **77**, 214101 (2008).
- [36] R. E. Rudd and J. E. Klepeis, Multiphase improved Steinberg-Guinan model for vanadium, *J. Appl. Phys.* **104**, 093528 (2008).
- [37] D. J. Weidner, Y. Wang, and M. T. Vaughan, Yield strength at high pressure and temperature, *Geophys. Res. Lett.* **21**, 753 (1994).
- [38] J. I. Langford, X-ray powder diffraction studies of vitromet samples, *J. Appl. Cryst.* **4**, 164 (1971).
- [39] L. Gerward, S. Morup, and H. Topsoe, Particle size and strain broadening in energy-dispersive x-ray powder patterns, *J. Appl. Phys.* **47**, 822 (1976).
- [40] J. Zhang, L. Wang, D. J. Weidner, T. Uchida, and J. Xu, The strength of moissanite, *Am. Mineral.* **87**, 1005 (2002).

- [41] L. Liu, H. X. Song, Z. Wang, H. Geng, Q. Jing, Y. Zhang, S. Liu, S. Xiang, Y. Bi, J. Xu, Y. Li, X. Li, and J. Liu, Strength and equation of state of fluorite phase CeO₂ under high pressure, *J. Appl. Phys.* **112**, 013532 (2012).
- [42] C. Prescher and V. B. Prakapenka, Dioptas: A program for reduction of two-dimensional x-ray diffraction data and data exploration, *High Press. Res.* **35**, 223 (2015).
- [43] P. M. Marcus and S. L. Qiu, Elasticity in crystals under pressure, *J. Phys.: Condens. Matter* **21**, 115401 (2009).
- [44] H. Wang, Y. C. Gan, H. Y. Geng, and X. R. Chen, MyElas: An automated tool-kit for high throughput calculation, post-processing and visualization of elasticity and related properties of solids, *Compt. Phys. Comput.* **281**, 108495 (2022).
- [45] G. Kresse and J. Furthmüller, Efficiency of *ab-initio* total energy calculations for metals and semiconductors using a plane-wave basis set, *Comput. Mater. Sci.* **6**, 15 (1996).
- [46] G. Kresse and J. Furthmüller, Efficient iterative schemes for *ab initio* total-energy calculations using a plane-wave basis set, *Phys. Rev. B* **54**, 11169 (1996).
- [47] P. E. Blöchl, Projector augmented-wave method, *Phys. Rev. B* **50**, 17953 (1994).
- [48] J. P. Perdew, K. Burke, and M. Ernzerhof, Generalized gradient approximation made simple, *Phys. Rev. Lett.* **77**, 3865 (1996).
- [49] L. Xiong and J. Liu, Structural phase transition, strength, and texture in vanadium at high pressure under nonhydrostatic compression, *Chin. Phys. B* **27**, 036101 (2018).
- [50] G. Grimvall, B. Magyar-Kope, V. Ozolins, and K. A. Persson, Lattice instabilities in metallic elements, *Rev. Mod. Phys.* **84**, 945 (2012).
- [51] A. Landa, J. Klepeis, P. Soderlind, I. Naumov, O. Velikokhatnyi, L. Vitos, and A. Ruban, Fermi surface nesting and pre-martensitic softening in V and Nb at high pressures, *J. Phys.: Condens. Matter* **18**, 5079 (2006).
- [52] J. D. Greiner, O. N. Carison, and J. F. Smith, Single-crystal elastic constants of vanadium and vanadium with oxygen additions, *J. Appl. Phys.* **50**, 4394 (1979).
- [53] S. Liu, Z. Li, Q. Jing, Y. Zhang, H. Ma, T. Tao, X. Wang, Y. Bi, J. Weng, and J. Xu, Note: A novel method to measure the deformation of diamond anvils under high pressure, *Rev. Sci. Instrum.* **85**, 046113 (2014).
- [54] Y. Yu, Y. Tan, C. Dai, X. Li, Y. Li, Q. Wu, and H. Tan, Phase transition and strength of vanadium under shock compression up to 88 GPa, *Appl. Phys. Lett.* **105**, 201910 (2014).
- [55] C. J. Wu, P. Söderlind, J. N. Glosli, and J. E. Klepeis, Shear-induced anisotropic plastic flow from body-centred-cubic tantalum before melting, *Nat. Mater.* **8**, 223 (2009).
- [56] D. Errandonea, B. Schwager, R. Ditz, C. Gessmann, R. Boehler, and M. Ross, Systematics of transition-metal melting, *Phys. Rev. B* **63**, 132104 (2001).
- [57] D. J. Steinberg, S. G. Cochran, and M. W. Guinan, A constitutive model for metals applicable at high-strain rate, *J. Appl. Phys.* **51**, 1498 (1980).
- [58] G. I. Taylor, The mechanism of plastic deformation of crystals, Part I. Theoretical, *Proc. R. Soc. London* **145**, 362 (1934).
- [59] F. R. N. Nabarro, Z. S. Basinski, and D. L. Holt, The plasticity of pure single crystals, *Adv. Phys.* **13**, 193 (1964).
- [60] H. Mughrabi, The α -factor in the Taylor flow-stress law in monotonic, cyclic and quasi-stationary deformations: Dependence on slip mode, dislocation arrangement and density, *Curr. Opin. Solid State Mater. Sci.* **20**, 411 (2016).
- [61] Z. C. Cordero, B. E. Knight, and C. A. Schuh, Six decades of the Hall-Petch effect—A survey of grain-size strengthening studies on pure metals, *Int. Mater. Rev.* **61**, 495 (2016).
- [62] Y. Zhao and J. Zhang, Enhancement of yield strength in zirconium metal through high-pressure induced structural phase transition, *App. Phys. Lett.* **91**, 201907 (2007).
- [63] A. K. Singh, A. Jain, H. P. Liermann, and S. K. Saxena, Strength of iron under pressure up to 55 GPa from x-ray diffraction line-width analysis, *J. Phys. Chem. Solids* **67**, 2197 (2006).
- [64] C. Meade and R. Jeanloz, Yield strength of B1 and B2 phase of NaCl, *J. Geophys. Res.* **93**, 3270 (1988).